Metabolic-imaging of human glioblastoma explants: a new precision-medicine model to predict tumor treatment response early

Mariangela Morelli[1**], Francesca Lessi[1], Serena Barachini[1], Romano Liotti[1], Nicola Montemurro[2], Paolo Perrini[2], Orazio Santo Santonocito[3], Carlo Gambacciani[3], Matija Snuderl[4], Francesco Pieri[3], Filippo Aquila[3], Azzurra Farnesi[3], Antonio Giuseppe Naccarato[5], Paolo Viacava[6], Francesco Cardarelli[7], Gianmarco Ferri[1,7], Paul Mulholland[8], Diego Ottaviani[8], Fabiola Paiar[9], Gaetano Liberti[2], Francesco Pasqualetti[9,10], Michele Menicagli[1], Paolo Aretini[1], Giovanni Signore[1], Sara Franceschi[1], Chiara Maria Mazzanti[1*]

1) Fondazione Pisana per la Scienza, Pisa, Italy.
2) Department of Neurosurgery, Azienda Ospedaliera Universitaria Pisana, Pisa, Italy.
3) Neurosurgical Department of Spedali Riuniti di Livorno, Livorno, Italy.
4) Department of Pathology, NYU Langone Medical Center, New York City, USA.
5) Department of Translational Research and New Technologies in Medicine and Surgery, University of Pisa, Italy.
6) Anatomy Pathology Department, Azienda Ospedaliera Toscana Nord-ovest, Livorno, Italy.
7) NEST, Scuola Normale Superiore and Istituto Nanoscienze-CNR, Pisa Italy.
8) Department of Oncology, University College London Hospitals, London, UK.
9) Department of Radiation Oncology, Azienda Ospedaliera Universitaria Pisana, University of Pisa, Italy.
10) Department of Oncology, University of Oxford, Oxford, UK.

The authors declare no potential conflicts of interest
* corresponding author
** co-corresponding author

Running title: A personalized cancer model to predict GB treatment response early
Funding: The work has been entirely financed by host institution Fondazione Pisana per la Scienza
Conflict of interest: There are no competing interests.
Authorship: conceived and designed the project, wrote the paper, analyze the data CMM; edited the paper, designed experiments, performed analyses, collected and analyzed data MM; performed experiments FL,SB, RL, SF; collected human materials NM,PP,OSS,CG,FrPi,FA,GL; pathological reports AGN,PV; clinical data, ethical approval FabPa,FPas,AF; idea conceptualization, paper editing, MS,PM,DO; data analysis PA; tissues processing MMe; FLIM methods optimizations GS,FC,GF.

Keywords: glioblastoma, predictive models, drug response, FLIM

Word count: 6500

Abstract

Background: Glioblastoma (GB) is the most severe form of brain cancer, with a 12-15 month median survival. Surgical resection, temozolomide (TMZ) and radiotherapy (RT) remain the primary therapeutic options for GB, and no new therapies have been introduced in recent years. This therapeutic standstill is primarily due to preclinical models that do not reflect the complexity of GB cell biology and fail to test anti-cancer treatments valuably. Better preclinical models for compound screening are therefore needed.

Methods: In-vitro 3D glioblastoma live explants (GB-EXPs) were derived from patients' resected tumors. We then applied metabolic imaging by fluorescence lifetime imaging microscopy (FLIM) on to GB-EXPs to assess drug response, using TMZ as our benchmark drug. Whole-transcriptome and whole-exome analyses were performed.

Results: Using FLIM we were able to stratify samples in Responder and Non-Responder tumors. Our functional precision medicine approach was successfully completed within 1 week of surgery. FLIM-based tumor samples stratification was well reflected at the molecular level, highlighting new targets associated with TMZ treatment and identifying a molecular signature associated with survival.

Conclusions: To the best of our knowledge, this is the first time that FLIM-based metabolic imaging is used on live glioblastoma 3D explants to test anti-neoplastic drugs rapidly. FLIM-based readouts of drug response in GB explants could improve precision treatment of patients with GB and the identification of new anti-GB drugs.

Keywords: glioblastoma, predictive models, drug response, FLIM

- Patients' tumors can be tested for several individual anti-cancer treatments early after surgery
- FLIM metabolic imaging is an accurate and rapid in vitro tumor treatment response assessment tool
- Our model can be exploited to identify new drug molecular targets and applied to other cancers

Importance of the study

In this article, we propose an accurate glioblastoma anti-cancer treatment response 3D-approach consisting of FLIM-based metabolic imaging applied directly to in-vitro vital patient-derived glioblastoma explants. Unlike other models, drug response of live explants is assessed within 1 week from patient's surgery, therefore with minimal tampering of natural tumor cyto-architecture, preventing the conventional structural and molecular divergence that the tumor undergoes after long time of in vitro culturing and with no animal involvement. This novel in vitro approach for glioblastoma treatment assessment could be exploited as a tool, in a range of clinical and laboratory settings to improve patients' clinical management. Selection of the optimal drug regimen for glioblastoma patients remains a clinical challenge and a method to assess the tumor specific response to several therapies at an early stage could be transformative

for glioblastoma patients' management. Furthermore, this model can be easily used for large-scale screening of new pharmaceutical compounds.

Introduction

Glioblastoma (GB) is the most common malignant primary brain tumor. Overall, the prognosis for patients with this disease is poor, with a 12-15 month median survival [1]. Maximal resection, temozolomide (TMZ) treatment and radiotherapy (RT) have remained the best option for several years [2]. The GB standard-of-care TMZ is a DNA-alkylating agent discovered in the 1970s and approved in 2005 by the FDA. The majority of responsive patients have O6-methylguanine DNA methyltransferase (MGMT) gene with methylated promoter and show higher survival rates than patients with hypo-methylated MGMT gene. Despite its low specificity, MGMT promoter status represents, today, the only clinical biomarker available to predict TMZ response [3].

Therefore, in this context, effective treatment options are a major unmet medical need. So far, conventional monolayer cell cultures have been widely used to test drug efficiency, although the lack of tissue architecture and complexity characteristic of this models fails to recapitulate the true biological processes in vivo. Recent advances in organoid technology revolutionized the in vitro culture tools for biomedical research by creating powerful 3D-dimensional models, but none fully captures the complexity of tumor biology and its microenvironment [4]. Because each GB tumor model has its shortcomings, there remains a need for better preclinical models for compound screening.

To overcome these limitations, we first developed a protocol to generate an in-vitro vital patient-derived IDH1/2 wild-type GB 3D model that we termed "glioblastoma explant" (GB-EXP), which, unlike other models [5] [6], is minimally handled and shortly grown in culture with no passaging in order to preserve the parental cyto-architecture. Then, to build a drug-response predictor tool, we combined NADH fluorescence lifetime imaging microscopy (FLIM) and the GB-EXP model to detect metabolic changes that are increasingly used to predict drug efficacy and to detect early responses to cancer treatment [7] [8] [9]. The intracellular metabolic cofactor NADH may be protein-bound or free in the cell, and these states affect its fluorescence decay, with bound NADH typically exhibiting longer lifetimes than free NADH. In cancer, metabolism shifts after treatment can be associated to an increase of NADH fluorescence lifetimes (increase of NADH bound/free ratio) as cells become less proliferative [10], showing a response to treatment. Thus FLIM of NADH represents a powerful non-invasive tool to monitor, in real time, the metabolic activities in living cells and tissues [7] [9]. To support this approach as an effective method of evaluating response to an anti-cancer treatment, we used TMZ as our benchmark drug, since it is the only approved drug used in GB and of which extensive knowledge has been achieved at the molecular level.

In this article we applied for the first time NADH-FLIM on in vitro vital GB patient-derived tumor explants with minimal tampering of natural tumor cytoarchitecture and with no animal involvement. This novel approach in GB treatment assessment could be exploited as a

tool for improving patient-tailored therapeutic strategy and for large scale screening of new pharmaceutical compounds.

Materials and methods

Human glioblastoma tissue collection

The study has been performed according to the declaration of Helsinki and the sample collection protocol was approved by the Ethics Committee of the University Hospital of Pisa (787/2015). Tumors were obtained from patients who underwent surgical resection of histologically confirmed GB after informed consent. Samples were obtained from the Neurosurgery Department of the "Azienda Ospedaliero-Universitaria Pisana" or from the Unit of Neurosurgery of Livorno Civil Hospital. A total of 16 patient cases from both male and female subjects were included in the present study. All cases had a diagnosis of GB with no previous history of any brain neoplasia and were not carrying R132 IDH1 or R172 IDH2 mutations. See supplementary methods for more information.

Glioblastoma Explant Cultures

The procedure used in this study to produce explants cultures is summarized in Figure. 1a. Fresh GB tumors or frozen samples, after a quick defrosting in a water bath at 37°C, were washed with DPBS in a sterile dish and cut with a scalpel into pieces <1 mm^2. Sample then were run on the gentleMACS Dissociator (Miltenyi Biotec) to mechanical dissociate them into 80 to 200 µm macrosuspensions, that were filtered through a 70-micron cell strainer to exclude smaller tissue pieces. Tissue suspensions were put in coverglass chamber slides (Nalge Nunc International), and then were covered with 300 ul of matrigel or in suspension. Cultures were placed in a 37°C, 5% CO2, and 90% humidity sterile incubator and grown for a maximum of 10/14 days with no passaging. GB-EXPs were cultured without additional growth factors to reduce additional tampering. Drug treatment started 3 days after GB-EXPs were cultured.
See supplementary materials for more information on 2D cell lines and 3D spheroids.

TMZ Drug treatments

The drug used in this study was TMZ (Sigma, St. Louis, MI, USA). U87 and T98G spheroids and patient-derived GB-EXPs were exposed to 600µM TMZ for 24hr, 48hr and 72hr for FLIM analysis, and for 1 week and 2 weeks for size and Ki67 mRNA analyses.
See supplementary materials for more information on 2D cell lines and 3D spheroids protocols.

Lifetime Imaging

Fluorescence lifetime imaging was performed with Olympus Fluoview 3000 confocal microscope using a 405 nm LDH-P-C-375B (Picoquant) excitation laser for NADH [11,12]. For control and treated samples, we acquired from 6 to 12 FLIM measurements each. Phasor approach was used to analyze NADH-FLIM data and was performed using the SimFCS suite as previously described [13]. Following the instructions reported in *"Two-component analysis of*

fractional NADH distribution" [13], we extrapolated from phasor plots the NADH free/bound fractional distribution curves of the controls and the treated samples, creating one mean distribution curve for controls and one for treated samples (Supplementary Figure 1S). To find differences between controls and treated NADH fractional distribution curves, for each of the 125 parts SimFCS dividing the curves a p-value was calculated using parametric Student t-test for each of the 125 parts dividing the curves, and fractions with p values <0.05 were considered significant. We calculated the percentage of response, considering only treated distribution, as: % of RESPONSE (%DR) = ∑SIGNIFICANT AREA/TOTAL AREA. Where: 1) the SIGNIFICANT AREA, is the area obtained by adding the areas of the histograms resulted to have a p-value<0.05, when compared with controls; 2) the TOTAL AREA is the area obtained by adding the areas of the 125 histograms. The %DR was calculated at 24, 48 and 72hr of treatment. The final %DR was obtained by calculating the weighted average (see supplementary materials).

Histology and stainings

Tissues and explants were fixed for 24 h, in 10% neutral-buffered formalin (Sigma-Aldrich) at room temperature. For immunofluorescence, CD105 polyclonal (Thermo Fisher, PA5-94980), CD3 monoclonal (F7.2.38) (Thermo Fisher, MA5-12577), Sox2 polyclonal (Thermo Fisher, 48-1400), GFAP monoclonal (ASTRO6) (Thermo Fisher, MA5-12023), GFAP polyclonal (Abcam, ab7260), Iba1 polyclonal (Wako 091-19741) primary antibodies were then applied at dilutions of 1:400, 1:20, 1:100, 1:100, 1:250, 1:1000, respectively overnight at 4 °C and visualized using Olympus Fluoview 3000 confocal microscope at a magnification of 60X, as above described.

Next-generation sequencing analyses

RNA-seq was performed using NextSeq 500 (Illumina, San Diego, CA, USA) for Next-Generation Sequencing. The library was prepared with Illumina Stranded Total RNA Prep with Ribo-Zero Plus kit (Illumina). Whole exome library preparation was performed using Illumina DNA Prep with Enrichment (Illumina, San Diego, CA, USA), following manufacturer procedure, starting from 500 ng of DNA. Sequencing was performed on NextSeq 500 (Illumina, San Diego, CA, USA) with 101 bp of reading length. See supplementary methods.

Statistical analysis

All summary data are presented as means ± s.d. All statistical analyses were performed in R and GraphPad Prism software (GraphPad 7.0). Sample size (n) values used for statistical analyses are provided in the text and supplementary materials. Individual data points are graphed or can be found in Source Data. Tests for differences between two groups were performed using Student's two-tailed unpaired t-test, as specified in the figure legends. No data points were excluded from the statistical analyses. Significance was set at $p < 0.05$. Linear discriminant analysis was performed with JMP10 software (SAS Institute).

Results

Tumor Samples

The dataset included 21 patient-derived surgery GB tissues, 5 of which consisted in the core and the periphery of the tumor from the same GB patient, obtained with the help of neuronavigation–guided microsurgical techniques. The age ranges from 30 to 80 years, patients include 10 males (62%) and 6 (38%) females. All tumor samples were derived from primary IDH1/2 wild-type GB samples as shown in Table 1S. MGMT methylation analysis revealed MGMT methylation discordancy between core (c) and peripheral (p) portions of samples GB3, GB4, GB6 and GB7 highlighting intra-tumor heterogeneity (Table 1S). In Table 2S are reported the pathological diagnosis and information about patients' therapeutic administrations.

In vitro culturing of patient-derived glioblastoma explants

We created in vitro a vital human GB patient-derived 3D system (Figure. 1a). Twenty one tumor pieces were first washed with PBS and specific lysis buffer in order to remove debris and red blood cells respectively (Figure 1b) and were immediately cultured by embedding them into matrigel (Figure 1c). GB tissues underwent, before culturing, a procedure of H&E staining and histological analysis, which was performed by an expert pathologist to confirm GB features (Figure 1d, Supplementary Figure 2S). GB-EXPs still showed active proliferation within 2 weeks in culture (Supplementary Figure 3S, Video 1S). To ensure vitality of GB-EXPs, we performed also live/dead cell viability assay (Figure 1e) and Ki67 immunohistochemistry (Figure 1f,g). In GB-EXPs, Ki67 expression analysis by immunohistochemistry, showed positivity at either 0 week or 2 weeks of culturing as shown in Figure 1f,g. The rate of proliferation was, furthermore, explored using Ki67 mRNA expression analysis (Figure 1h) and size analysis (Figure1i,j), that showed a slight gradual increase of proliferation rate over time, specifically from 0 week, to 2 weeks, confirming the studies reported in the literature for other culturing approaches[5]. To assess whether GB-EXPs maintain the cyto-composition of parental tumors, we further characterized and explored cellular diversity between surgery GB tissues and GB-EXPs by choosing a panel of GB markers including GFAP (astrocytes), IBA1 (microglia), SOX2 (stem cells), CD105 (endothelial cells) and CD3 (lymphocytes). The immunofluorescence assays on GB-EXPs showed the presence of each individual cell type indicating retention of parental architecture including vasculature features and lymphocytes (Figure 1k,l).

FLIM metabolic-imaging approach validation in known glioblastoma *in vitro* systems

Initially, to validate the efficacy of our FLIM-based metabolic-imaging approach we assessed it on two 2D (Supplementary Figure 4S) and 3D GB cell lines systems known already to be TMZ responsive and non-responsive. To mimic the GB-EXPs 3D structures, we produced TMZ responder 3D-U87 and TMZ non-responder 3D-T98G spheroids and measured the impact of TMZ drug response on FLIM metabolic imaging data. In the literature, several TMZ dilutions ranging from 1μM to 1mM were studied on GB organoids [14] with the most effective doses between 250μM and 1mM. In line with these results, we chose a dosage of 600μM. FLIM data was acquired at 72hr on a total of 10 spheroids, with characteristic dimension in the 70-200 μm range, for each experimental condition. In Figure 2a,c representative images of a spheroid

is shown including brightfield images (top row) and NADH-FLIM phasor map (on the bottom) colored in accordance to the color bar defined on the side. Color-bar defines the metabolic path from NADH in the bound state (red/magenta) to NADH in the free state (green/white) as explained in material and methods section (Supplementary Fig 1S a,b). According to the phasor-based FLIM data analysis we obtained a NADH fractional distribution curve of free and bound NADH molecules for each image (Supplementary Fig 1S a,b), that identifies a metabolic signature that goes from an oxidative phosphorylation phenotype with low free/bound NADH fractions to a glycolytic phenotype with high free/bound NADH[15]. In Figure 2b,d we report the fractional NADH mean distribution curves of control and TMZ treated 3D-U87 (Figure 2b) and 3D-T98G spheroids (Figure 2d). The difference between the two curves was expressed as a percentage of drug response (%DR) calculated considering the area of the significant histograms (in green, Figure 2b,d) out of the total histograms area under the treated GB-EXPs curve (see materials and methods section). After 72hr of TMZ exposure in responsive 3D-U87 spheroids, treated fractional NADH mean curve, showed a statistically significant shifts towards higher fractions of NADH bound molecules when compared to controls (see Figure 2b), as demonstrated by a 55%DR and as already reported for the 2D system. As previously discussed this indicates an increase in the oxidative metabolism typical of a lesser proliferative state [16 7 9]. The %DR is shown by green histograms in Figure 2b and is reflected in the phasor map of a representative spheroid as shown in Figure 2a,c.
To support the FLIM results, we performed spheroid-size measurements over time, using a dedicated software (OrganoSeg) [17]. Control and TMZ treated spheroids for both cell lines were followed for two weeks after treatment and photographed at 0, 1 and 2 weeks. A representative brightfield image of a 3D-U87 and 3D-T98G spheroid at each time point is shown in Figure 2e,f together with the matched area size image for both experimental conditions (control and treated). The area size measurement of the 3D-U87 images at each time point revealed a statistically significant increase in size for the control spheroids (n=12) (p-value=0.03, Student's t test) while, as expected, a statistically significant decrease was detected for the TMZ treated ones (n=12) (1week, p-value=0.003 and 2 weeks p-value<0.00002, respectively, Student's t test) (Figure 2g). In 3D-T98G a statistically significant increase in size was recorded at 1 and 2 weeks for both control (n=12) (p-value=0.0001, Student's t-test) and TMZ treated spheroids (n=12) (p-value=0.001, p-value<0.00002, respectively, Student's t test), confirming their resistance to TMZ treatment (Figure 2h). Ki67 real-time expression analysis at 2 weeks after TMZ treatment confirms FLIM readouts and size results (p-value=0.002. Student's t test) (Fig 2i.).

FLIM metabolic imaging of TMZ treated patient-derived GB-EXPs

Using the methodological criteria set by the supporting technical experiments on 2D- and 3D-systems, we assessed TMZ response in 21 GB tumors. For each patient's tumor GB-EXPs were chosen of similar dimensions between 70 and 200μm for drug testing and a minimum of 14 to a maximum of 33 explants were analyzed (Table 4S). The GB-EXPs of the tumor case in Figure 3a show overlapping fractional NADH mean distribution curves between the treated (red) and control (blue) explants, which is indicative of an identical distribution of bound and free NADH[9]

(Figure 3b) with a 0%DR. In Figure 3c,d we report examples of GB-EXPs, derived from GB15 case, resulted to have distinctive phasor maps and NADH fractional mean distribution curves, distinguishable between controls and treated cases. The distribution curves (Figure 3e,f) showed a statistical significant shift of the red curves towards more abundant bound NADH molecular species in TMZ treated explants compared to the control ones, with a 59.3%DR (Figure 3e) and 90.9%DR (Figure 3f), corresponding to 24 and 72hrs TMZ treatment, respectively (Table 5S). Higher amounts of bound-state NADH reflects an oxidative metabolism, which is typical of less proliferative cells [10 7] and therefore of a responsive tumor.
Overall to asses a final annotation of TMZ Responder (Resp) or Non Responder (Non-Resp) we calculated for each case a Final %DR to TMZ treatment (see materials and method), as shown in Figure 3g (green-red color scale) leading us to the stratification of our tumor samples in 11 Non-Resp (%DR<5) and 10 Resp, furtherly subdivided into several categories consisting of Low Responders (LR) (5≤%DR<20), Medium Responders (MR) (20≤%DR<50) and High Responders (HR) (%DR≥50) (Figure 3g). It is noteworthy to point out that between core and peripheral portions of the 5 GB tumor cases included in the dataset, we observed a different drug response behavior (Supplementary Figure 5S). As expected, GB2, GB3 and GB4 core regions show a more drug resistant behavior compared to peripheral portions [18] in particular GB2c was assessed as MR and GB2p as HR, while GB3c/4c were NR and GB3p/4p were LR. GB6c/p and GB7c/p were both assessed as Non-Resp (Figure 3g).
To corroborate FLIM-based metabolic imaging drug efficacy predictions in stratifying samples in Resp and Non-Resp, we performed size analysis on all 21 sample-derived GB-EXPs. We acquired images at 0, 1 and 2 weeks for both control and TMZ treated cases for a minimum of 15 to a maximum of 81 GB-EXPs per sample (Table 4S). The examples reported in Figure 3h show a clear decrease in size for the Resp GB-EXP compared to the Non-Resp one. Overall the area measurement of the GB-EXPs Resp group revealed a statistically significant decrease at 1 and 2 weeks after TMZ treatment ($p=0.0002$; $p<0.0001$, respectively; Student's t test thus supporting FLIM-based metabolic imaging predictions (Figure 3i).
To further support our results, we measured changes in Ki67 mRNA expression 2 weeks after TMZ treatment. Differential analysis of Ki67 expression was performed on 7 Non-Resp and 8 Resp samples. Ki67 mRNA expression was statistically reduced in the Resp group after TMZ treatment compared to controls, indicating a lower proliferation rate ($p=0.003$, Student's t test). (Figure 3j). No difference was found in the Non-Resp group.
In accordance with what is reported in the clinic and in the literature [19], we observed a higher percentage of methylated cases (77%) in the Resp tumor group compared to the Non-resp tumor group (45%) (Figure 3k).

Genome-wide analyses

We performed next generation sequencing analyses to characterize the genetic background of the Resp and Non-Resp tumors in order to establish a correlation between the TMZ response phenotype identified by our FLIM approach and the underlying molecular profile.

Whole Transcriptome Analysis (WTA)

WTA was performed on 9 Resp and 9 Non-Resp samples including the cases provided with a core and a peripheral portion. Differential expression analysis identified 42 statistically significant genes between the two experimental groups (Table 6S). In Figure 4a a heatmap analysis was initially run excluding the peripheral tumor portions to avoid repeated measures derived from similar genetic background with core counterparts. Results show 7 Resp and 7 Non-Resp samples perfectly clustered on the bases of the 42 gene expression levels, supporting that distinct TMZ responsive and non-responsive phenotypes are well reflected at the molecular level. Among the 42 genes (Table 6S), we identified several genes involved in TMZ response that are worthy to be mentioned. Our results are confirmed by the upregulation of CA9 in the Non-Resp group, whose inhibition enhances the sensitivity of glioma cells to TMZ, and highlights the value of developing drugs against the CA9 pathway, for combination therapy with TMZ [20](Table 9S, Fig 5a). In the Non-Resp group we identified down-regulation of the FGFR3 gene, associated with poor response to TMZ treatment[21]. Most noteworthy are the genes that we report in Fig. 5b, BIRC3 and NDRG2, which show a differential gene expression that varies gradually according to %DR supporting phasor-FLIM drug response stratification. Some studies in 2016 and 2021[22] [23] report that BIRC3 gene was found expressed at higher level in recurrent GB than in newly diagnosed GB and emerged as a novel driver of TMZ therapeutic resistance, suggesting that, during TMZ therapy, concurrent BIRC3-specific inhibition could be exploited for enhanced benefit. The NDRG2 gene has the opposite trend compared to the BIRC3 gene (Fig. 5b). The main mechanism that underlies NDRG2 silencing in glioma is unknown. There is also a debate whether NDRG2 gene activity reflects on survival of glioma patient [24]. Furthermore, we identified two genes completely silenced in all samples of the Non-Resp group, such a ANKRD28 and PTPRD (Figure 4a,b). While the ANKRD28 gene has unknown role in GB, the tyrosine phosphatase PTPRD is a tumor suppressor that is frequently inactivated and mutated in GB and other human cancers [25].

Lastly, on the 42 significant genes we performed a stepwise discriminant analysis that enabled the identification of a 17 gene signature (Table 6S), which could discriminate the Resp and Non-Resp tumor samples with a 100% accuracy (Figure 4c,d). To investigate a potential disease course of the patients whose tumors we predicted the TMZ response, we decided to query the TCGA database consisting of hundreds of clinically and molecularly fully characterized GB patients. Therefore, the 17 gene profile was used in the "SurvExpress Biomarker Validation of Cancer Gene Expression" tool, to interrogate an extended TCGA-derived GB patient population (n=146). A non-parametric statistics, used to estimate the survival function from lifetime data of the 146 cases, produced a Kaplan Meier plot identifying a Low and High Risk Survival group, as shown in Figure 4e,f, whose molecular profile corresponded to the Resp and Non-Resp tumor groups respectively (Figure 4f). As shown in Figure4e, it is noteworthy to highlight that the Resp gene expression profile is associated exclusively to the patients that belong to the group of the longest survivors (>50 months).

To establish the type of GB molecular subtype to which our samples belong, we exploited a TCGA 490 gene expression profile, deposited by the Anderson Cancer Center, and created a classifier that allowed the assignment of each sample to one of the Mesenchymal, Classical, Proneural, Neural and G-CIMP categories. As shown in Figure 4g the Non-Resp group was

composed mostly by samples of the Mesenchymal kind, which represents the most aggressive subtype[26] (Table 7S).

Whole Exome Analysis (WEA)

WEA was evaluated in 16 GB tumors divided in 9 Non-Resp and 7 Resp cases. The mutational landscape of Resp vs Non-Resp is shown in Figure 5a,b. In Non-Resp samples the mutational load is higher for any type of variant than in Resp cases (Figure 5a) as widely described in more aggressive and less TMZ-responsive tumor phenotypes[27].
We analyzed mutations in genes known to be altered in IDH1-WT GB by referring to My Cancer Genome-MCG (mycancergenome.org database). We found 14 mutated genes in the 16 GB cases for a total of 28 different variants (Figure 5c, Supplementary Figure 6S, Table 8S). The analysis confirmed a higher mutational burden in the Non-Resp group with more deleterious alteration in the PTEN, RB1 and NF1 gene, which are well known tumor suppressor genes in GB [28]. Using Maftools forestPlot we identify seven genes significantly distinguishing the two groups of tumors (Figure 5d, Supplementary Figure 7S and Table 9S).
CNApp[29] analysis was used to analyze the chromosomal alterations of the 16 GB samples (Figure 5e,f). More than 50% of the samples in both the Resp and Non-Resp groups, have alterations of chromosomes 7, 9 and 10, specifically characteristic of IDH-WT GBs[30]. The Non-Resp tumors show loss of chromosome 14, already described in GB patients as carrier of several tumor suppressor genes[31], unlike the Resp group (Figure 5e,f). In Resp group increased gain of chromosome 19 and 20 is observed, identified as being a favorable prognostic marker in GB[32]. These results are indicative of a differential genetic background associated with FLIM-based TMZ response assessement, further confirming the goodness of our approach.

Discussion

Glioblastoma is the most aggressive malignant tumor of the central nervous system, with a highly unfavorable prognosis. Novel experimental approaches have shown limited success to improve patient survival due to several underlying factors, such as aggressive and highly infiltrative growth, inter-patient and intra-tumoral heterogeneity and multiple resistance mechanisms[33]. To address these limitations, 3D cancer models were implemented, providing a more robust patient-specific approach despite several shortcomings [4]. Here we, developed a novel rapid functional precision medicine approach to establish a tumor specific response after drug treatment, consisting in applying NADH-FLIM on our in vitro vital patient-derived GB 3D model, termed GB-EXP, minimally handled and tested within a 1 week after surgery, representing at best the pathological condition in vivo. Our in vitro 3D model demonstrates that microglia, stem cells, vascular endothelial cells, including lymphocytes persist, and that these cultures retain cyto-architectural of parental tumors.

Currently, traditional methods for establishing response to treatment can be evaluated using a variety of biological, molecular, genetic and chemical assays [34]. Many of these tests

require a long and laborious procedural time which in the long term alters an already formed 3D tumor structure such as a GB-EXP exemplifies.

Studying the intracellular metabolic shifts allows to see changes in cellular behavior early because it predates any actual proliferation [8]. In several recent studies, measurements of cancer-cell metabolism by live-imaging using intrinsic fluorescence from metabolic enzymatic cofactors have shown promise as a sensitive non-invasive method for early predicting drug response[7] [35]. Therefore NADH FLIM turns out to be perfectly suitable to GB-EXPs since it identifies metabolic changes rapidly and non-invasively on the biological material used, leaving it vital [7] without interfering with its internal structure. Therefore, GB-EXP model represents an attractive suitable platform for patient-specific drug testing.

Consequently, as fast as 72 hr post-TMZ treatment, it was possible to classify all 21 GB tumors, in Resp or Non-Resp cases. We confirmed the results also by the conventional procedures (size and Ki67 mRNA analyses). All Resp cases under TMZ chemotherapeutic treatment showed an increase in amount of bound NADH, stemming from a shift of cellular metabolism from glycolysis (more proliferative state) toward oxidative phosphorylation (less proliferative state) [35 9 10 16].

Interestingly, we measured the MGMT methylation status in GB samples and found, as expected, a higher percentage of methylated cases in the Resp group. Although the MGMT methylation status is accepted as a prognostic biomarker in predicting patient response to TMZ treatment, inconsistencies do occur and currently challenge the efficacy of this biomarker in clinical practice, raising the question of its value[3].

Furthermore, we investigated the gene expression and mutational profile of the Resp and Non-Resp groups. Here, it is essential to highlight that the approach we used, albeit on a small case study, has allowed us to identify two phenotypically different tumor populations that carry their own distinct molecular profile. Such a distinction at the molecular level strengthen the accuracy of the present approach. In fact, between the two groups of patients, who share many common characteristics of the GB, we have been able to highlight, quite strikingly, markers already described in the literature, but also new potential targets associated with the response to TMZ such as ANKRD28, PTPRD, ZNF713, DNAH5, SLC7A4, GALNTL5, FBN3, DENND6B and OTOR. Moreover, a unique 17-gene signature significantly discriminating the Resp and Non-Resp tumors emerged and significantly correlated to a Low and High Risk Survival group in a TCGA fully clinically characterized GB population. Further studies are needed to investigate the potential role of the 17 gene signature in glioblastoma.

To the best of our knowledge, this study is the first to apply FLIM-based metabolic imaging on in vitro vital patient-derived GB tumors to perform a non-invasive treatment tumor response assessment early before losing parental tumor architecture. The lack of predictive biomarkers is a major limitation in GB clinical oncology and, as of today, clinicians urgently need step-changing informative tools to support their decision-making therapy approaches. A method to predict patients' tumor specific drug response before the onset of the therapy can be transformative for GB patients' management. The performance of such functional precision medicine approach can provide additional information regarding patient's tumor vulnerabilities. These functional approach opens the door to new discoveries and generates further knowledge of the disease, which in turn will increase the likelihood of producing useful

therapeutic solutions [36]. It is important to point out that the full promise of precision medicine in oncology has yet to be realized, as more individuals may benefit from functional approaches. We envision, in the glioblastoma clinical field, an increasing implementation of functional precision medicine protocols and a transition from therapeutic approaches followed by watchful waiting, to informed decisions based on specific patient-derived GB-EXPs treatment-response predictions. This approach can therefore be seen also as a way to test new FDA-approved anticancer drugs in vitro directly on the tumor and could also be seen as a springboard for new drugs that need to be transferred to the more advanced stages of clinical trials.

Acknowledgements

We would like also to express our special thanks to Mr. Raffaele Cotugno for his kind donation to this project.

Bibliography

1. Tan AC, Ashley DM, López GY, Malinzak M, Friedman HS, Khasraw M. Management of glioblastoma: State of the art and future directions. *CA Cancer J Clin*. 2020;70(4):299-312. doi:10.3322/caac.21613
2. Maher EA, Bachoo RM. *Glioblastoma*.; 2014. doi:10.1016/B978-0-12-410529-4.00078-4
3. Butler Madison, Pongor Lorinc, Su Yu-Ting, Xi Liqiang, Raffeld Mark, Quezado Martha, Trepel Jane, Aldape Kenneth, Pommier Yves WJ. MGMT Status as a Clinical Biomarker in Glioblastomaitle. *Trends Cancer*. 2020;6(5):380-391.
4. Pinto B, Henriques AC, Silva PMA, Bousbaa H. Three-dimensional spheroids as in vitro preclinical models for cancer research. *Pharmaceutics*. 2020;12(12):1-38. doi:10.3390/pharmaceutics12121186
5. Jacob F, Salinas RD, Zhang DY, et al. A Patient-Derived Glioblastoma Organoid Model and Biobank Recapitulates Inter- and Intra-tumoral Heterogeneity. *Cell*. 2020;180(1):188-204.e22. doi:10.1016/j.cell.2019.11.036
6. Darrigues E, Zhao EH, De Loose A, et al. Biobanked glioblastoma patient-derived organoids as a precision medicine model to study inhibition of invasion. *Int J Mol Sci*. 2021;22(19). doi:10.3390/ijms221910720
7. Lukina MM, Dudenkova V V., Ignatova NI, et al. Metabolic cofactors NAD(P)H and FAD as potential indicators of cancer cell response to chemotherapy with paclitaxel. *Biochim Biophys Acta - Gen Subj*. 2018;1862(8):1693-1700. doi:10.1016/j.bbagen.2018.04.021
8. Kolenc OI, Quinn KP. Evaluating cell metabolism through autofluorescence imaging of NAD(P)H and FAD. *Antioxidants Redox Signal*. 2019;30(6):875-889. doi:10.1089/ars.2017.7451
9. Datta R, Heaster TM, Sharick JT, Gillette AA, Skala MC. Fluorescence lifetime imaging microscopy: fundamentals and advances in instrumentation, analysis, and applications. *J Biomed Opt*. 2020;25(07):1. doi:10.1117/1.jbo.25.7.071203
10. Trinh AL, Chen H, Chen Y, et al. Tracking functional tumor cell subpopulations of malignant glioma by phasor fluorescence lifetime imaging microscopy of NADH. *Cancers (Basel)*. 2017;9(12):1-13. doi:10.3390/cancers9120168
11. Erkkilä MT, Reichert D, Gesperger J, et al. Macroscopic fluorescence-lifetime imaging of

NADH and protoporphyrin IX improves the detection and grading of 5-aminolevulinic acid-stained brain tumors. *Sci Rep*. 2020;10(1). doi:10.1038/s41598-020-77268-8
12. Ludtmann MHR, Angelova PR, Zhang Y, Abramov AY, Dinkova-Kostova AT. Nrf2 affects the efficiency of mitochondrial fatty acid oxidation. *Biochem J*. 2014;457(3):415-424. doi:10.1042/BJ20130863
13. Ranjit S, Malacrida L, Jameson DM, Gratton E. Fit-free analysis of fluorescence lifetime imaging data using the phasor approach. *Nat Protoc*. 2018;13(9):1979-2004. doi:10.1038/s41596-018-0026-5
14. Golebiewska A, Hau AC, Oudin A, et al. *Patient-Derived Organoids and Orthotopic Xenografts of Primary and Recurrent Gliomas Represent Relevant Patient Avatars for Precision Oncology*. Vol 140. Springer Berlin Heidelberg; 2020. doi:10.1007/s00401-020-02226-7
15. Skala MC, Riching KM, Bird DK, et al. In vivo Multiphoton Fluorescence Lifetime Imaging of Proteinbound and Free NADH in Normal and Pre-cancerous Epithelia. *J Biomed Opt*. 2007;12(2):1-19. doi:10.1117/1.2717503.In
16. Arteaga CL, Skala MC. Metabolism Predicts Drug Response in Breast Cancer. 2015;74(18):5184-5194. doi:10.1158/0008-5472.CAN-14-0663.Quantitative
17. Borten MA, Bajikar SS, Sasaki N, Clevers H, Janes KA. Automated brightfield morphometry of 3D organoid populations by OrganoSeg. *Sci Rep*. 2018;8(1):1-10. doi:10.1038/s41598-017-18815-8
18. Bastola S, Pavlyukov MS, Yamashita D, et al. Glioma-initiating cells at tumor edge gain signals from tumor core cells to promote their malignancy. *Nat Commun*. 2020;11(1):1-17. doi:10.1038/s41467-020-18189-y
19. Radke J, Koch A, Pritsch F, et al. Predictive MGMT status in a homogeneous cohort of IDH wildtype glioblastoma patients. *Acta Neuropathol Commun*. 2019;7(1):89. doi:10.1186/s40478-019-0745-z
20. Xu X, Wang Z, Liu N, et al. Association between SOX9 and CA9 in glioma, and its effects on chemosensitivity to TMZ. *Int J Oncol*. 2018;53(1):189-202. doi:10.3892/ijo.2018.4382
21. Kipper FC, Silva AO, Marc AL, et al. Vinblastine and antihelmintic mebendazole potentiate temozolomide in resistant gliomas. *Invest New Drugs*. 2018;36(2):323-331. doi:10.1007/s10637-017-0503-7
22. Wang D, Berglund A, Kenchappa RS, Forsyth PA, Mule JJ, Etame AB. BIRC3 is a novel driver of therapeutic resistance in Glioblastoma. *Sci Rep*. 2016;6(October 2015):1-13. doi:10.1038/srep21710
23. Frazzi R. BIRC3 and BIRC5: multi-faceted inhibitors in cancer. *Cell Biosci*. 2021;11(1):0-14. doi:10.1186/s13578-020-00521-0
24. Skiriute D, Steponaitis G, Vaitkiene P, et al. Glioma malignancy-dependent NDRG2 gene methylation and downregulation correlates with poor patient outcome. *J Cancer*. 2014;5(6):446-456. doi:10.7150/jca.9140
25. Veeriah S, Brennan C, Meng S, et al. The tyrosine phosphatase PTPRD is a tumor suppressor that is frequently inactivated and mutated in glioblastoma and other human cancers. *Proc Natl Acad Sci U S A*. 2009;106(23):9435-9440. doi:10.1073/pnas.0900571106
26. Zhang P, Xia Q, Liu L, Li S, Dong L. Current Opinion on Molecular Characterization for GBM Classification in Guiding Clinical Diagnosis, Prognosis, and Therapy. *Front Mol Biosci*. 2020;7(September):1-13. doi:10.3389/fmolb.2020.562798
27. Wang L, Ge J, Lan Y, et al. Tumor mutational burden is associated with poor outcomes in diffuse glioma. *BMC Cancer*. 2020;20(1):1-12. doi:10.1186/s12885-020-6658-1
28. McDonald KL, Tabone T, Nowak AK, Erber WN. Somatic mutations in glioblastoma are

associated with methylguanine-DNA methyltransferase methylation. *Oncol Lett*. 2015;9(5):2063-2067. doi:10.3892/ol.2015.2980
29. Franch-Expósito S, Bassaganyas L, Vila-Casadesús M, et al. CNApp, a tool for the quantification of copy number alterations and integrative analysis revealing clinical implications. *Elife*. 2020;9. doi:10.7554/eLife.50267
30. Mirchia K, Sathe AA, Walker JM, et al. Total copy number variation as a prognostic factor in adult astrocytoma subtypes. *Acta Neuropathol Commun*. 2019;7(1):92. doi:10.1186/s40478-019-0746-y
31. Hu Jie, Jiang Chengchuan, HoKeung NG, Pang Jesse C S TCYK. Chromosome 14q may harbor multiple tumor suppressor genes in primary glioblastoma multiforme. *Chin Med J*. 2002;115(8):1201-4.
32. Geisenberger C, Mock A, Warta R, et al. Molecular profiling of long-term survivors identifies a subgroup of glioblastoma characterized by chromosome 19/20 co-gain. *Acta Neuropathol 2015 1303*. 2015;130(3):419-434. doi:10.1007/S00401-015-1427-Y
33. Aldape K, Brindle KM, Chesler L, et al. Challenges to curing primary brain tumours. *Nat Rev Clin Oncol*. 2019;16(8):509-520. doi:10.1038/s41571-019-0177-5
34. Hughes JP, Rees SS, Kalindjian SB, Philpott KL. Principles of early drug discovery. *Br J Pharmacol*. 2011;162(6):1239-1249. doi:10.1111/j.1476-5381.2010.01127.x
35. Walsh Alex J., Cook Rebecca S., Sanders Melinda E. AL, CilibertoGennaro, ArteagaCarlos L. SC. Quantitative optical imaging of primary tumor organoid metabolism predicts drug response in breast cancer. *Cancer Res*. 2014;74(18):5184–5194.
36. Letai A, Bhola P, Welm AL. Functional precision oncology: Testing tumors with drugs to identify vulnerabilities and novel combinations. *Cancer Cell*. 2022;40(1):26-35. doi:10.1016/j.ccell.2021.12.004

Figure 1 GB-EXPs cultures*(a) Experimental design. (b) A surgery tumor sample. (c) GB-EXP embedded in matrigel. (d) H&E staining of a surgery GB tissue. (e) Live/dead staining of a GB-EXP at 2 weeks after culturing. (f-g) Ki67 immunostaining of GB-EXPs in suspension at 0 week and 2 weeks. (h) Ki67 mRNA expression analysis of 13 GB case-derived GB-EXPs at 0 and 2 weeks. Graph represents mean ± s.d. of triplicated measures. (i) Representative brightfield and area size images of a GB-EXP in matrigel at 0 week, 1 week and 2 weeks. (j) Size analysis 20 GB case-derived GB-EXPs at 0, 1 and 2 weeks. (k-l) Immunofluorescence assays of surgery GB tissue (k) and GB-EXPs (l). GFAP (astrocytes), IBA1 (microglia), SOX2 (stem cells), CD105 (endothelial cells) and CD3 (lymphocytes).* ***Abbreviations****: WTA, Whole Transcriptome Analysis; WEA, Whole Exome Analysis; FC, Flow Cytometry; H&E, Hematoxylin and Eosin; MGMT, MGMT promoter methylation analysis.*

Figure 2 ***FLIM-based metabolic imaging in 3D-U87 and 3D-T98G****. (a,c) Representative images of 3D-U87 (a) and 3D-T98G (c) controls and treated cells, subdivided in brightfield images of a spheroid and the corresponding phasor map. (b,d) NADH fractional mean distribution curves of controls (blue) and treated cells (red) of 3D-U87 (b) and 3D-T98G cells (d). (e,f) Representative size analysis images of 3D-U87 (e) and 3D-T98G (f). (g) Size analysis of 3D-U87 (h) Size analysis of 3D-T98G cells. (i) Ki67 mRNA expression at 2 weeks.*

Figure 3 FLIM-based metabolic imaging on GB-EXPs*. (a,c,d) A Non-Resp and two Resp tumor derived GB-EXPs 72 hrs post-treatment are shown including a brightfield image and the corresponding phasor map. (b) Non-Resp tumor fractional NADH mean distribution curves. (e,f) Resp tumor fractional NADH mean distribution. (g) %DR at 24, 48, and 72 hr, represented with a grey scale is shown for each GB case. The annotation of Resp and Non-Resp was assigned on the basis of the Final %DR (red-green scale). (h) GB-EXP size analysis images. (i) Size analysis of Controls, Resp and Non-Resp patients-derived GB-EXPs (n=215, n=130, n=124 respectively) at 1 and 2 weeks. (j) Ki67 mRNA expression analysis (k) MGMT promoter methylation status in Resp (n=9) and Non Resp (n=11) cases.*

Figure 4 Gene expression profiling of GB-EXPs*. (a) RNASeq heatmap. (b) Expression levels of 4 genes in GB tumors subdivided in HR, MR, LR and NR. (c) Stepwise discriminant analysis (d) PCA showing RNAseq data of 17 DE genes. (e) The 17 gene panel Kaplan Meier plot. Concordance*

Index = 64.34, Log−Rank Equal Curves p=0.001853, R^2=0.192/0.998 Risk Groups Hazard Ratio = 1.79 (conf. int. 1.23 ~ 2.6), p=0.002172. (f) Expression levels of the 17 genes in TCGA database and in GB tumors. (g) GB Molecular subtypes.

Figure 5 Mutational profiling of GB-EXPs*. (a,b) Mutation landscape of GB cohort (n=16). (c) Co-bar plot of the most frequently gene mutations in GB. (d) Co-bar plot of the genes significantly discriminating Non-Resp and Resp groups. (e) CNApp frequencies for the p and q arms of each chromosome in Resp and Non-Resp groups.*

Figure1

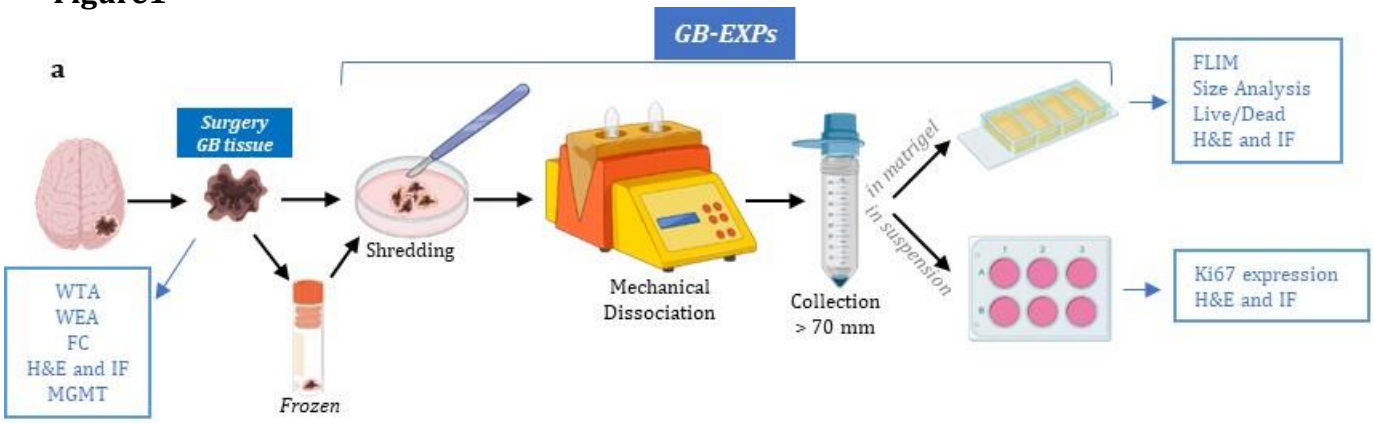
GB-EXPs
a
Surgery
GB tissue
WTA
WEA
FC
H&E and IF
MGMT
Frozen
Shredding
Mechanical
Dissociation
Collection
> 70 mm
in matrigel
in suspension
FLIM
Size Analysis
Live/Dead
H&E and IF
Ki67 expression
H&E and IF

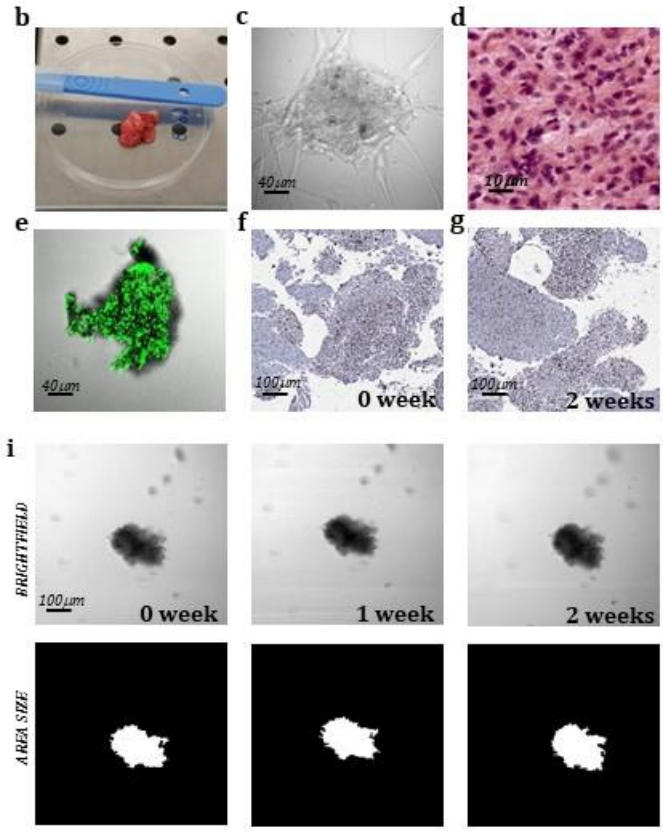
b
c
d
e
f
g
40µm
10µm
40µm
100µm
0 week
100µm
2 weeks
i
BRIGHTFIELD
AREA SIZE
100µm
0 week
1 week
2 weeks

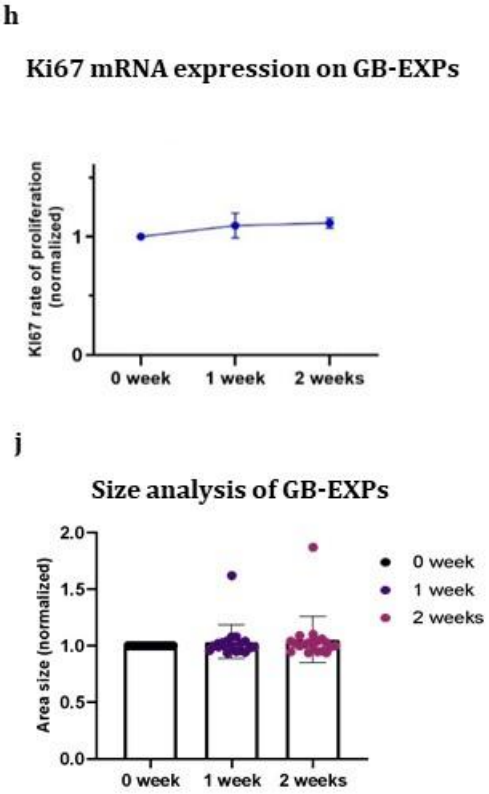
h
Ki67 mRNA expression on GB-EXPs
Ki67 rate of proliferation
(normalized)
1
0
0 week
1 week
2 weeks
j
Size analysis of GB-EXPs
Area size (normalized)
2.0
1.5
1.0
0.5
0.0
0 week
1 week
2 weeks

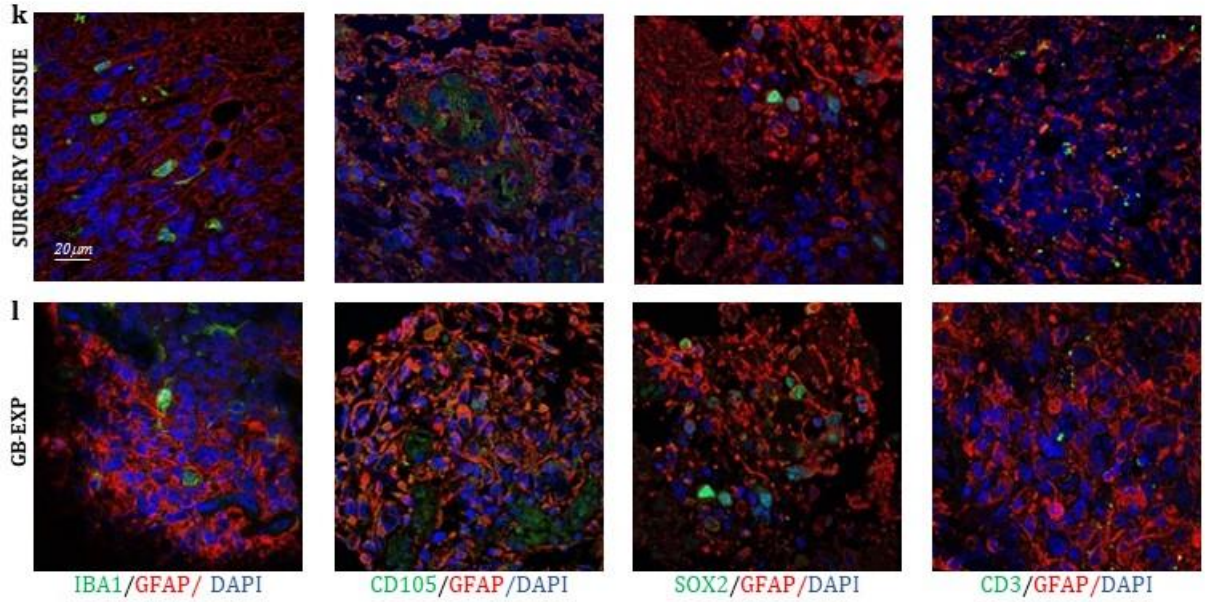
k
SURGERY GB TISSUE
20µm
l
GB-EXP
IBA1/GFAP/ DAPI
CD105/GFAP/DAPI
SOX2/GFAP/DAPI
CD3/GFAP/DAPI

Figure 2

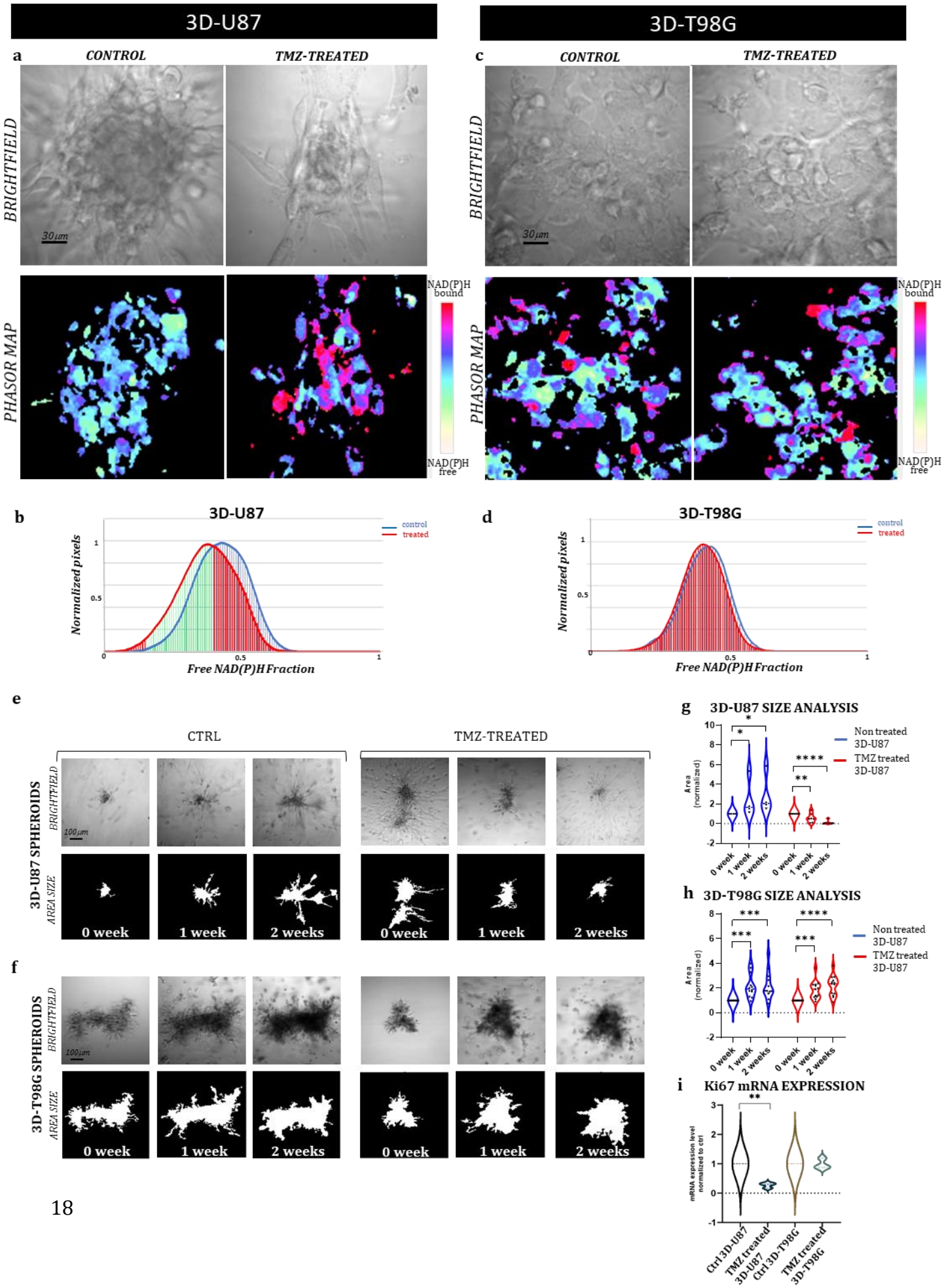
3D-U87
3D-T98G
a
CONTROL
TMZ-TREATED
BRIGHTFIELD
30µm
PHASOR MAP
NAD(P)H bound
NAD(P)H free
c
b
3D-U87
Normalized pixels
Free NAD(P)H Fraction
control
treated
d
3D-T98G
e
CTRL
TMZ-TREATED
3D-U87 SPHEROIDS
AREA SIZE
100µm
0 week
1 week
2 weeks
f
3D-T98G SPHEROIDS
g
3D-U87 SIZE ANALYSIS
Area (normalized)
Non treated 3D-U87
TMZ treated 3D-U87
h
3D-T98G SIZE ANALYSIS
i
Ki67 mRNA EXPRESSION
mRNA expression level normalized to ctrl
Ctrl 3D-U87
TMZ treated 3D-U87
Ctrl 3D-T98G
TMZ treated 3D-T98G

Figure 3

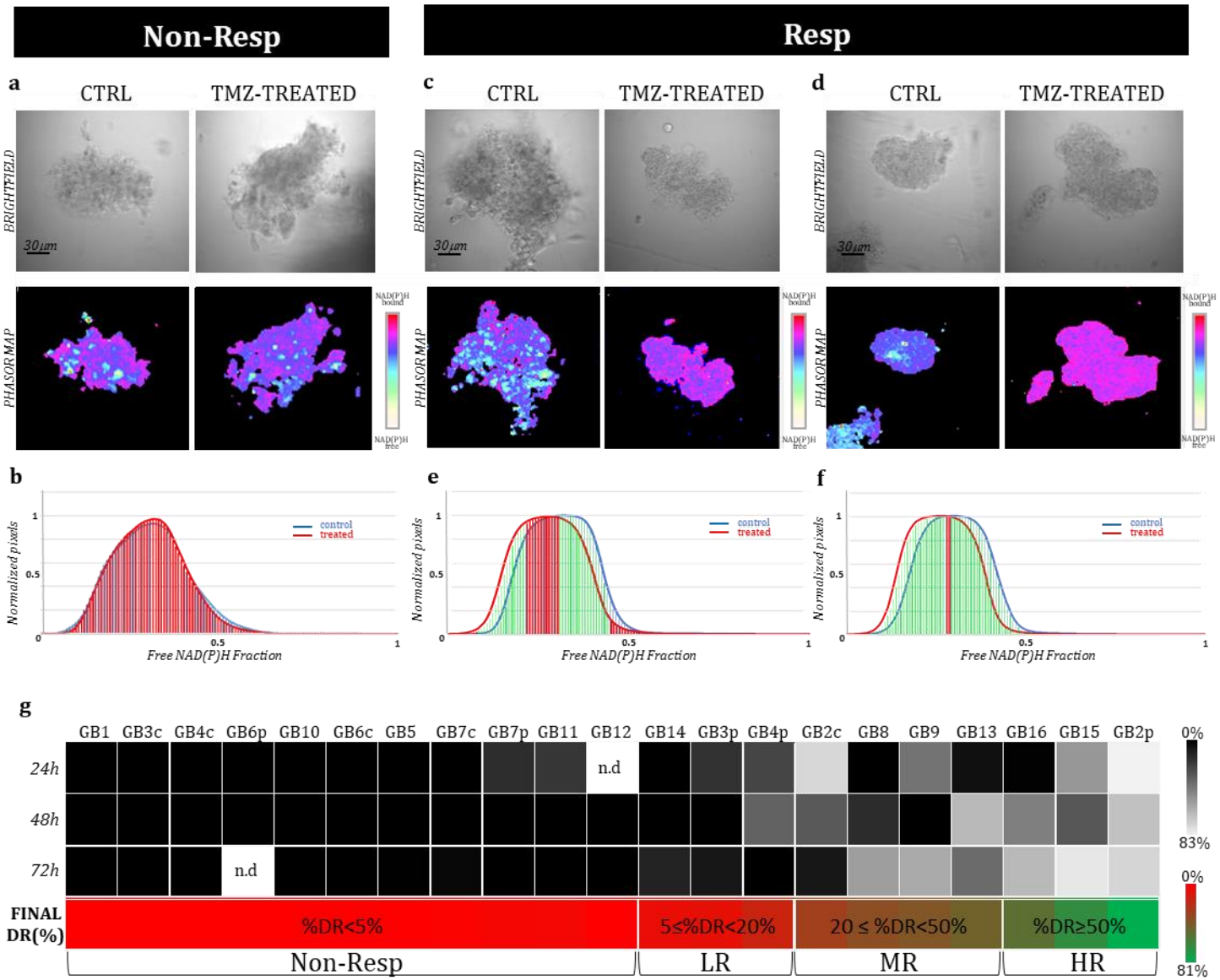
Non-Resp
Resp
a
CTRL
TMZ-TREATED
c
CTRL
TMZ-TREATED
d
CTRL
TMZ-TREATED
BRIGHTFIELD
30µm
PHASOR MAP
NAD(P)H bound
NAD(P)H free
b
e
f
Normalized pixels
control
treated
Free NAD(P)H Fraction
g
GB1 GB3c GB4c GB6p GB10 GB6c GB5 GB7c GB7p GB11 GB12 GB14 GB3p GB4p GB2c GB8 GB9 GB13 GB16 GB15 GB2p
24h
48h
72h
n.d
0%
83%
FINAL DR(%)
%DR<5%
5≤%DR<20%
20 ≤ %DR<50%
%DR≥50%
Non-Resp
LR
MR
HR
81%

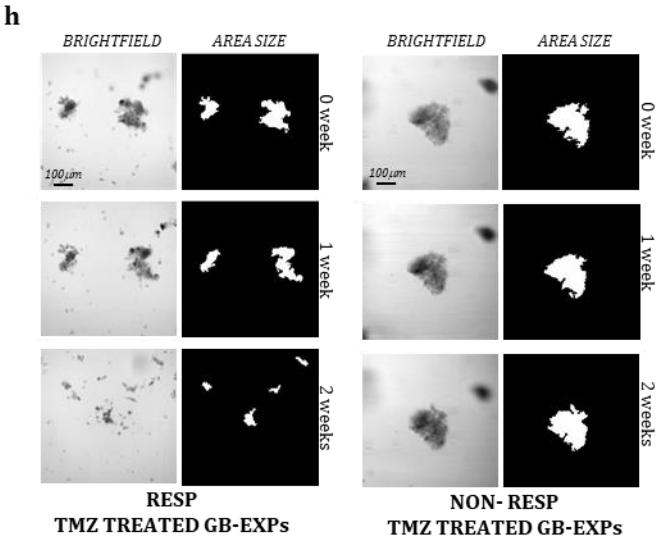
h
BRIGHTFIELD
AREA SIZE
100µm
0 week
1 week
2 weeks
RESP
TMZ TREATED GB-EXPs
NON- RESP
TMZ TREATED GB-EXPs

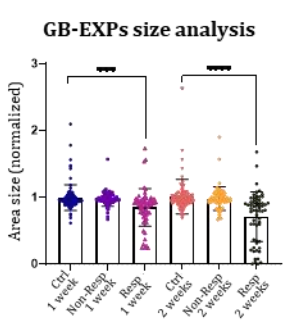
i
GB-EXPs size analysis
Area size (normalized)
Ctrl 1 week
Non-Resp 1 week
Resp 1 week
Ctrl 2 weeks
Non-Resp 2 weeks
Resp 2 weeks

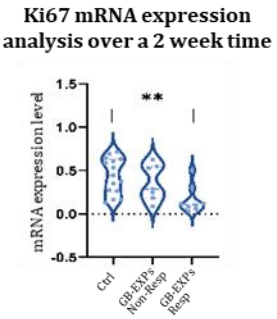
j
Ki67 mRNA expression analysis over a 2 week time
mRNA expression level
Ctrl
GB-EXPs Non-Resp
GB-EXPs Resp

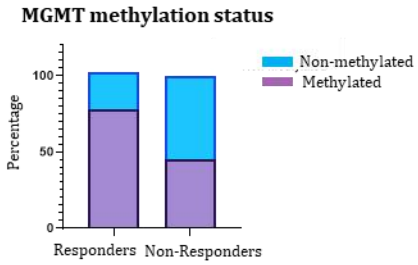
k
MGMT methylation status
Non-methylated
Methylated
Percentage
Responders
Non-Responders

Figure 4

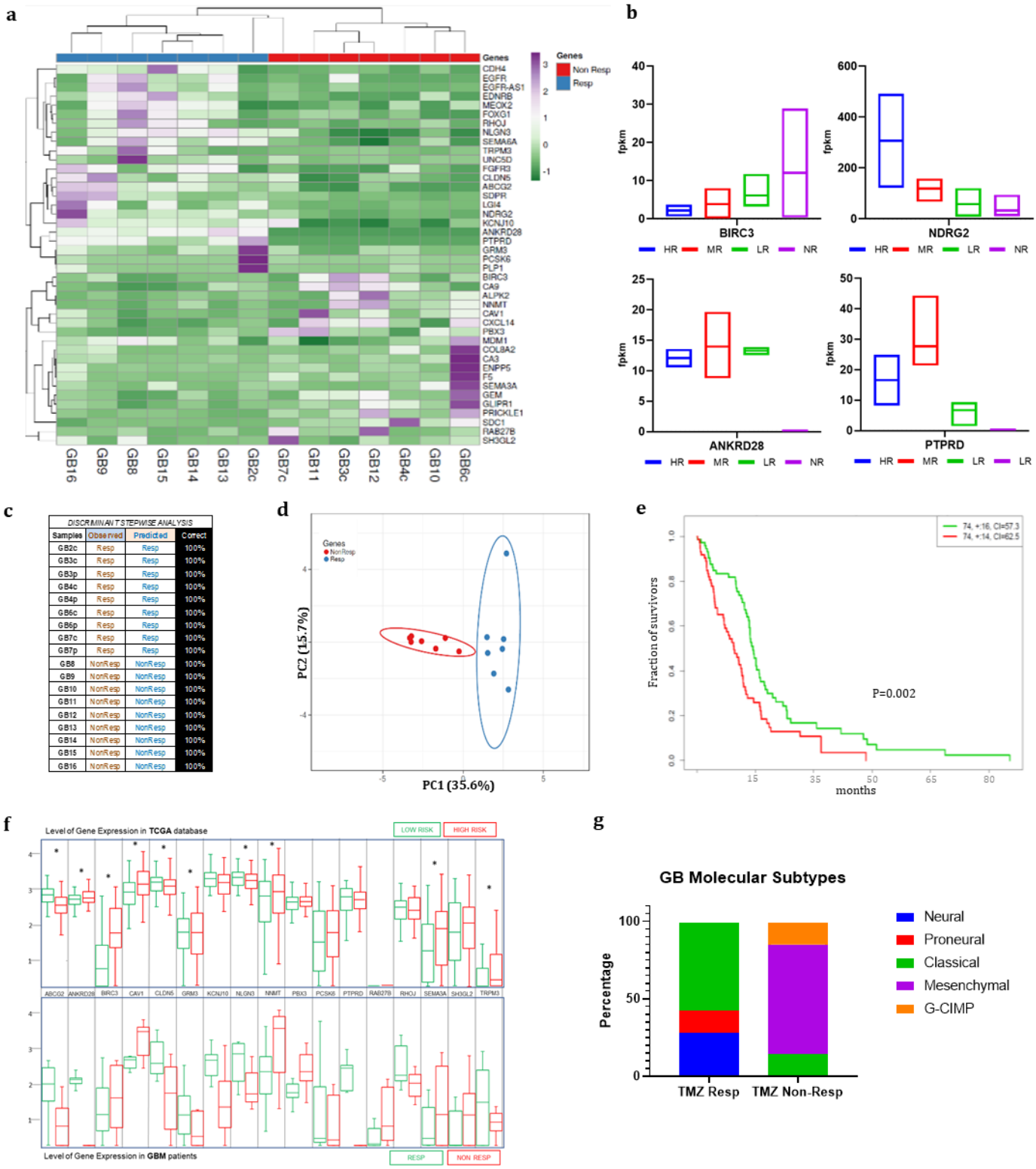
a
Genes
Non Resp
Resp
CDH4
EGFR
EGFR-AS1
EDNRB
MECK2
FOXG1
RHOJ
NLGN3
SEMA6A
TRPM3
UNC5D
FGFR3
CLDN5
ABCG2
SDPR
LGI4
NDRG2
KCNJ10
ANKRD28
PTPRD
GRM3
PCSK6
PLP1
BIRC3
CA9
ALPK2
NNMT
CAV1
CXCL14
PBX3
MDM1
COL8A2
CA3
ENPP5
F5
SEMA3A
GEM
GLIPR1
PRICKLE1
SDC1
RAB27B
SHOGL2
GB16
GB9
GB8
GB15
GB14
GB13
GB2c
GB7c
GB11
GB3c
GB12
GB4c
GB10
GB6c
b
fpkm
BIRC3
NDRG2
ANKRD28
PTPRD
HR
MR
LR
NR
c
DISCRIMINANT STEPWISE ANALYSIS
Samples | Observed | Predicted | Correct
GB2c | Resp | Resp | 100%
GB3c | Resp | Resp | 100%
GB3p | Resp | Resp | 100%
GB4c | Resp | Resp | 100%
GB4p | Resp | Resp | 100%
GB6c | Resp | Resp | 100%
GB6p | Resp | Resp | 100%
GB7c | Resp | Resp | 100%
GB7p | Resp | Resp | 100%
GB8 | NonResp | NonResp | 100%
GB9 | NonResp | NonResp | 100%
GB10 | NonResp | NonResp | 100%
GB11 | NonResp | NonResp | 100%
GB12 | NonResp | NonResp | 100%
GB13 | NonResp | NonResp | 100%
GB14 | NonResp | NonResp | 100%
GB15 | NonResp | NonResp | 100%
GB16 | NonResp | NonResp | 100%
d
Genes
NonResp
Resp
PC2 (15.7%)
PC1 (35.6%)
e
Fraction of survivors
P=0.002
months
f
Level of Gene Expression in TCGA database
LOW RISK
HIGH RISK
Level of Gene Expression in GBM patients
RESP
NON RESP
g
GB Molecular Subtypes
Percentage
TMZ Resp
TMZ Non-Resp
Neural
Proneural
Classical
Mesenchymal
G-CIMP

Figure 5

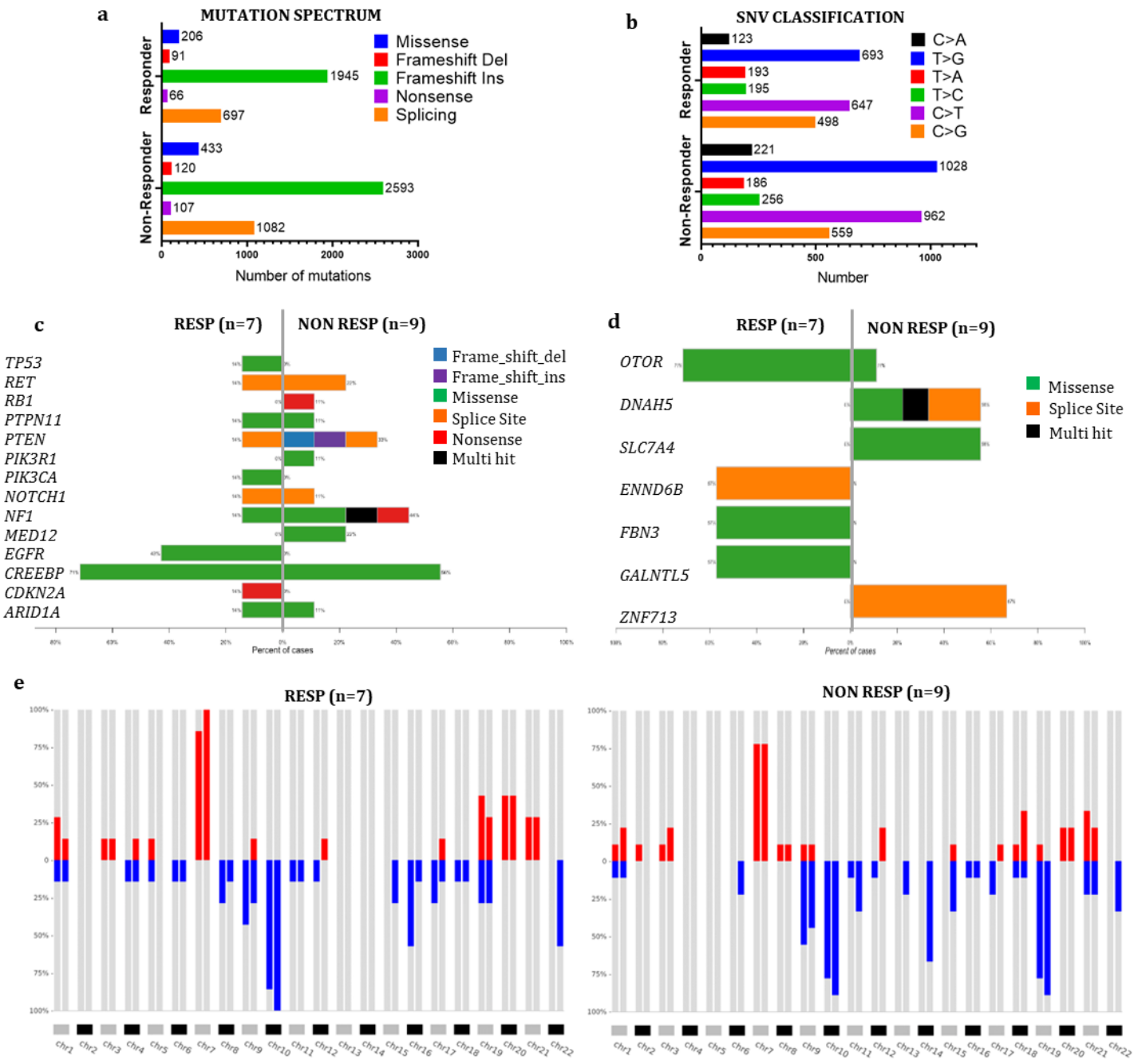
a
MUTATION SPECTRUM
Responder
Non-Responder
206
91
1945
66
697
433
120
2593
107
1082
Missense
Frameshift Del
Frameshift Ins
Nonsense
Splicing
0
1000
2000
3000
Number of mutations
b
SNV CLASSIFICATION
Responder
Non-Responder
123
693
193
195
647
498
221
1028
186
256
962
559
C>A
T>G
T>A
T>C
C>T
C>G
0
500
1000
Number
c
RESP (n=7)
NON RESP (n=9)
TP53
RET
RB1
PTPN11
PTEN
PIK3R1
PIK3CA
NOTCH1
NF1
MED12
EGFR
CREEBP
CDKN2A
ARID1A
Frame_shift_del
Frame_shift_ins
Missense
Splice Site
Nonsense
Multi hit
Percent of cases
d
RESP (n=7)
NON RESP (n=9)
OTOR
DNAH5
SLC7A4
ENND6B
FBN3
GALNTL5
ZNF713
Missense
Splice Site
Multi hit
Percent of cases
e
RESP (n=7)
NON RESP (n=9)
100%
75%
50%
25%
0
chr1
chr2
chr3
chr4
chr5
chr6
chr7
chr8
chr9
chr10
chr11
chr12
chr13
chr14
chr15
chr16
chr17
chr18
chr19
chr20
chr21
chr22